Published in final edited form as:
Heart Rhythm. 2014 September ; 11(9): 1584–1591. doi:10.1016/j.hrthm.2014.05.013.

Body surface localization of left and right atrial high-frequency rotors in atrial fibrillation patients: A clinical-computational study

Miguel Rodrigo, MS[*], **María S. Guillem, PhD**[*], **Andreu M. Climent, PhD**[†], **Jorge Pedrón-Torrecilla, MS**[*], **Alejandro Liberos, MS**[*], **José Millet, PhD**[*], **Francisco Fernández-Avilés, MD, PhD**[†], **Felipe Atienza, MD, PhD**[†], and **Omer Berenfeld, PhD, FHRS**[‡]

[1]Bio-ITACA, Universitat Politécnica de Valencia, Valencia, Spain

[2]Cardiology Department, Hospital General Universitario Gregorio Marañón, Instituto de Investigación Sanitaria Gregorio Marañón, Madrid, Spain

[3]Center for Arrhythmia Research, University of Michigan, Ann Arbor, Michigan

Abstract

BACKGROUND—Ablation is an effective therapy in patients with atrial fibrillation (AF) in which an electrical driver can be identified.

OBJECTIVE—The aim of this study was to present and discuss a novel and strictly noninvasive approach to map and identify atrial regions responsible for AF perpetuation.

METHODS—Surface potential recordings of 14 patients with AF were recorded using a 67-lead recording system. Singularity points (SPs) were identified in surface phase maps after band-pass filtering at the highest dominant frequency (HDF). Mathematical models of combined atria and torso were constructed and used to investigate the ability of surface phase maps to estimate rotor activity in the atrial wall.

RESULTS—The simulations show that surface SPs originate at atrial SPs, but not all atrial SPs are reflected at the surface. Stable SPs were found in AF signals during 8.3% ± 5.7% vs 73.1% ± 16.8% of the time in unfiltered vs HDF-filtered patient data, respectively ($P < .01$). The average duration of each rotational pattern was also lower in unfiltered than in HDF-filtered AF signals (160 ± 43 ms vs 342 ± 138 ms; $P < .01$), resulting in 2.8 ± 0.7 rotations per rotor. Band-pass filtering reduced the apparent meandering of surface HDF rotors by reducing the effect of the atrial electrical activity occurring at different frequencies. Torso surface SPs representing HDF rotors during AF were reflected at specific areas corresponding to the fastest atrial location.

Address reprint requests and correspondence: Dr María S. Guillem, Bio-ITACA, Universidad Politécnica de Valencia, Camino de Vera sn, 46022 Valencia, Spain. *Or*, Dr. Felipe Atienza. Cardiology Dept, Hospital Gregorio Marañón, C/Dr. Esquedo, 46, 28007 Madrid, Spain. mguisan@eln.upv.es; fatienza@secardiologia.es.

None of the companies disclosed financed the research described in this article.

CONCLUSION—Phase analysis of surface potential signals after HDF filtering during AF shows reentrant drivers localized to either the left atrium or the right atrium, helping in localizing ablation targets.

Keywords

Atrial fibrillation; Electrocardiography; Mapping; Atrial rotor; Body surface potential mapping

Introduction

Recent invasive[1, 2] and noninvasive[3–6] mapping studies of human atrial fibrillation (AF) have demonstrated a variety of spatiotemporal patterns of activation, including high-frequency sites, rotors, and focal discharges during human AF. Arguably, the identification of the AF mechanism in each patient may help selecting the best therapy or ablation strategy to deliver to that individual patient. However, how to map effectively and determine the specific mechanisms of AF maintenance in individual patients is still elusive.[7]

It has recently been shown that noninvasive mapping allows the identification of high dominant frequency (DF) atrial sources during human AF.[5] However, the ability of surface mapping data to determine the specific activation patterns underlying the fast activation that characterize AF (ie, focal vs reentrant activity) has not been studied before. The aim of this study was to investigate the potential use of surface mapping recordings for the estimation of propagation patterns during AF on an individual patient basis.

Methods

Patients and body surface potential recording

The 14 patients included in this study were admitted for ablation of drug-refractory paroxysmal and persistent AF (see Online Supplemental Table 1). All patients gave informed consent. The protocol was approved by the institutional ethics committee. In patients arriving in sinus rhythm, AF was induced by electrical burst pacing.

Intracardiac electrograms (EGMs) were sequentially obtained from both atria during the procedure.[5] The power spectral density of EGMs was computed to determine the local DFs in each atrium.

Surface electrocardiograms (ECGs) were recorded simultaneously with the intracardiac EGMs using a grid of 67 electrodes on a vest covering the torso (see Online Supplemental Figure 1A). Ventricular activation was removed by administering a central venous bolus of adenosine (12–18 mg), and 4-second segments of surface ECGs surrounding the longest RR interval were used for the analysis. Acquired surface potentials on the entire torso were baseline subtracted and low-pass filtered at 30 Hz.[3] The power spectral density of all signals was computed to determine the local DFs and their distribution on the body surface.[5]

Surface ECGs were then filtered at the highest dominant frequency (HDF) found on the torso surface or at the highest DF found at either left atrial EGMs (left atrial highest dominant frequency [LA-HDF]) or right atrial EGMs (right atrial highest dominant

frequency [RA-HDF]) by using a 2-Hz bandwidth band-pass filter (see the Online Supplement).

Computational models of the atria and torso

To guide processing and interpretation of the recorded body surface potentials, we simulated the electric potentials behavior on a computerized model of the atria within the torso during different impulse propagation patterns. This approach will enable investigating for the first time the manifestation of atrial reentrant activity on both the internal volume and the torso surface. We constructed a generic atria-torso model consisting of a spherical shell of active tissue, representing the atria, within a passive torso modeled as a uniform volume conductor bounded by a spherical surface with no-flux conditions (see the Online Supplement).

The electric potential resulting from the wave propagation simulated on the atrial sphere was studied everywhere on 20 concentric spheres by using the boundary element method.[8] The potentials on the external sphere, defined as the torso surface, and in the internal layers were analyzed to characterize the time course of the potential distribution everywhere; in particular, the patterns and time course of the filaments resulting from atrial rotors were characterized.

Phase singularity and filaments

Phase maps on the torso surface of patients and in each concentric layer in the computer models were obtained from the potential phase signal of each node by using the Hilbert transform.[9] A *singularity point* (SP) was defined as the point in a phase map that is surrounded by phases from 0 to 2π. Only those SPs that were present for the duration of at least 1 full rotation were considered (see the Online Supplement).

A *filament* was defined as the connection between SPs across spherical layers at a given time. Only filaments that complete at least 1 rotation on the outermost surface were considered.

Statistical analysis

The *t* test was used to evaluate the statistical significance between continuous paired or unpaired variables, and statistical significance was considered for $P < .05$. All data are reported as mean ± SD.

Results

Surface mapping of atrial activity during AF

Surface phase maps of the unipolar voltage time series recorded during AF show unstable patterns, as can be appreciated by the transient SPs seen in the maps from a sample patient presented in Figure 1A, as opposed to stable rotational patterns observed during atrial flutter (see Online Supplemental Figure 1). Long-lasting SPs were rarely observed during AF without band-pass filtering, and those observed tended to drift erratically large distances in short time. However, after band-pass filtering of the potential signal around the HDF (6.8 Hz), surface phase maps showed more stable SPs for the same AF episode (Figure 1A). In

Figure 1B, the arrows connecting sequential activations in ECGs recorded around the SP in Figure 1A show a clear reentrant pattern, which, after HDF filtering, transformed into long-lasting rotational patterns with stable SPs. Considering data from all patients, stable SPs were found in unfiltered AF signals during 8.3% ± 5.7% of the time vs 73.1% ± 16.8% after HDF filtering of signals ($P < .01$). The average SP duration concomitantly increased after HDF filtering (160 ± 43 ms vs 342 ± 138 ms; $P < .01$). Of the average HDF of 9.2 ± 2.3 Hz for body surface potential mapping or 9.3 ± 2.0 Hz for EGM, the latter corresponds to an average of 2.9 ± 0.7 continuous rotations per SP observed in our cohort of patients. Many observed SPs drift and appear or disappear on the borders of the surface mapped area or at the beginning and end of the periods analyzed; thus, this average number of rotations represents a lower limit for their life span. Indeed, Figure 1C and Online Movie 1 show a rotor in the middle of the mapped area at the beginning of the period analyzed, which, after about 1400 ms, disappears at the lower boundary of the area. After a period of fuzzy SP behavior in the posterior torso (see Online Movie 1) for about 330 ms, an SP appears and remains in the mapped area for the rest of the analyzed period. This case shows that the actual life span of rotors could be longer than the conservative average life span we calculate. Further evidence of atrial rotor drifting is provided by the simultaneous EGM recorded at the highest DF site (Figure 1E), which is unstable in intervals 1–4 and monomorphic at interval 4–5, which is consistent with the observed drifting on the torso surface.

Simulations to understand band-pass filtering of AF patterns at the HDF

The finding that the dynamics of the body surface SPs dramatically depends on HDF filtering raises questions regarding the phase map interpretation. Unfortunately, the ability to simultaneously collect electrical data in the atria and inside the torso volume and surface to make inferences between atrial activity and its manifestation on the body surface is limited, leading us to rely on computer simulations for guidance.

In Figure 2A, simulation with an LA-RA model and the multisphere torso model is depicted. In this model, there is a single functional rotor in the LA hemisphere turning at 7.2 Hz while the RA hemisphere is passively activated at a lower frequency (3.9 Hz). Figure 2A shows the phase maps of 3 concentric layers between the epicardium (left) and the torso surface (right) at various times. The phase maps become smoother toward the torso surface, reflecting the low-pass filter effect of the passive torso volume on the extracellular potentials. In the epicardial layer, there is 1 stable SP at the location of the functional rotor (LA) that appears at similar positions in the outer layers and another SP at the less stable wavebreak location at the interface between the faster LA and the slower RA. The azimuth and elevation of SPs detected on the surface are not preserved across layers, and so the filament arising from the LA rotor exhibits a deflection in its trajectory to the torso. The deflection angle of the filaments before HDF filtering is not stationary over time, and instead, the filament trajectory describes a cone. However, Figure 2B shows that HDF filtering significantly reduces the filaments' deflection and stabilizes them to follow a straight path from the epicardium to the surface. We hypothesize that HDF filtering minimized the effect of the atrial activity that is not activated at the HDF and thus stabilized the filament. To corroborate such hypothesis, we sum all the RA dipoles into a single equivalent dipole and plot its vector projection on the RA-LA interface (YZ) plane (Figure

2C). In addition, we plot the trajectory of the external SP originated by the LA rotor projection on the same (YZ) plane. In Figure 2D, we observe the match in the time course and rotation frequency between the RA equivalent dipole rotation and the SP trajectory. Accordingly, we conclude that SPs arising at the LA-RA interface as a consequence of abrupt changes in propagation direction that reached the outermost layer disappear after HDF filtering since their activation frequencies did not match with the HDF. In addition, we observe that a mirror filament appears in opposite direction and with chirality as compared with the true rotor originating at the SP on the LA epicardium. Indeed, after the attenuation of RA activation frequencies, potentials on the RA hemisphere are caused by the rotating electrical activity on the LA and observed from a contralateral point of view (see Online Supplemental Figure 2).

We further explore the behavior of filaments under more complex wave patterns; in Figure 3, we analyze simulation results from a 50% LA-50% fibrotic area model. In this case, epicardial activity consists of an LA rotor with a stable SP and a disorganized activity with several unstable SPs in the fibrotic area (Figure 3A). In Figure 3B, most of the filaments originate at SPs involving a small piece of fibrotic tissue but do not originate at the driving rotor. As can be seen, spatial smoothing stabilizes filaments and eliminates all but a single filaments' pair reaching the surface. To understand how the filaments originating at the epicardium disappear inside the torso, we color coded them according to the chirality of the SPs. Figure 3C clearly shows that filaments are continuous and do not vanish inside the passive volume conductor; rather, a filament does not reach the surface once it joins its counterrotating neighbor. Overall, that mutual cancellation of filament pairs reduces the average number of SPs at increasing distances from the epicardium (Figure 3D). At the outermost layer, only 2 SPs can be observed: one which is the "true" SP and another that we term the "mirror" SP and appears after the extinction of SPs at the fibrotic area and extension of the stable LA rotor filament to the contralateral aspect of the torso. Mutual cancellation of filaments can indeed result in a failure to detect "true" SPs originating at small atrial areas (see Online Supplemental Figure 3), an effect that may be counteracted by HDF filtering.

Indeed, the discrimination between true and mirror rotors can be performed on the basis of the spectral properties of surface recordings at the HDF. In Figure 4A, we show a surface phase map with 2 SPs that resulted from HDF filtering of simulation with only 1 stable rotor. The SP labeled T is the end point of the filament that connects directly to the epicardial SP (hence the label "true" SP); the SP labeled M is the surface end point of a filament originating at the epicardial wall contralateral to the stable rotor (hence the term "mirror" SP; see Online Supplemental Figure 2). On the phase map, these SPs seem indistinguishable; however, the spectral power at the rotor frequency band is maximal at the true SP. Figure 4B shows a similar analysis in a patient. The patient's surface phase map shows 2 SPs, and the traces below the map show that while in 1 SP location the maximal power is at the HDF, in the other SP the power at that frequency is much less, indicating that the former is the true SP and the latter is the mirror SP.

Centers of rotational activity in human AF

True SPs detected, defined as those with at least 60% of their spectral content at the HDF band (Figure 4), tended to concentrate at certain torso areas related with the DF distribution in the atria.[5] The trajectory of a surface SP that drifted during 2 seconds on the posterior torso of a patient after LA-HDF filtering (band-pass filtering at the HDF found in simultaneous left intracardiac EGM recordings) is depicted in Figure 5A (see Online Movie 1, from t = 1850 to t = 3850). The trajectory of a surface SP that drifted during 500 ms on the right anterior torso of another patient after RA-HDF filtering is shown in Figure 5B (see Online Movie 2). In Figure 5C, the 2-dimensional histogram of "true" SP locations after LA-HDF filtering in patients with an interatrial DF gradient > 1 Hz (n = 10) shows a predominant location of SPs on the posterior torso. The 2-dimensional histogram of true SP locations after RA-HDF filtering in patients with an interatrial DF gradient shows a predominant localization on the right anterior torso (Figure 5D). The locations of the maximum numbers of true LA or RA SPs (dark red regions) are shown in Figures 5C and 5D to reside well within the areas demarcated by the HDFs originating at either the LA or the RA, respectively, on the basis of our previous surface-atrial DF distribution correlation study.[5]

Discussion

In this study, we show that phase maps of surface potentials during AF after HDF filtering allow observing reentrant patterns with spatiotemporal stability. In contrast, the unfiltered surface phase maps display unstable reentrant patterns. The short-lived and unstable surface reentrant activity in the nonfiltered data is suggested by computer simulations to result from the superposition of irregular electrical activity at frequencies other than the HDF, which may mask the presence of the more stable reentrant activation.

Rotors and AF maintenance in humans

Circus propagation was proposed as a possible mechanism for the perpetuation of AF as early as in the 1920s[10] and gained relevance after experimental demonstration of functional rotors maintaining AF by optical mapping in isolated sheep heart preparations.[11] However, some studies continue advocating for the alternative mechanism of multiple wavelets as the predominant mechanism underlying AF maintenance.[12] In humans, evidence for stable rotors as a mechanism of AF maintenance was until recently sporadic and indirect[13] as well as questionable.[14] Narayan et al[2] reported that rotor activity is detectable by panoramic intra-cardiac mapping in approximately 70% of the 98 of 101 patients with AF and brief ablation at the centers of those rotors was effective in terminating or slowing the arrhythmia. Although the interpretation of mapping and ablation results obtained with the basket catheter are still somewhat controversial,[7] they constitute strong evidence for the major role of rotors in maintaining AF. The results presented in this study are consistent with the latter evidence: the body surface potential mapping is detecting rotor activity also in approximately 70% of the time during AF. However, our study further demonstrates that the rotor activity is the fastest activity in the patients we studied.

Noninvasive identification of rotors in human AF

Previous high-density surface mapping of atrial propagation patterns showed that the presence of surface reentries was infrequent and accounted for few consecutive rotations.[3, 4] Results from our mathematical simulations suggest that the ability of raw surface potentials in detecting existing rotors is compromised by (1) the organization degree of areas activated at lower rates than did the rotor and (2) the amount of myocardial tissue activated at the same rate as the rotor. Interestingly, computer simulations demonstrate that the far-field effect of areas with low organization could produce less distortion on SP torso projection than could areas with higher organization. However, activity of rotors covering a small atrial portion may be masked by the electrical activity of the rest of the atria, even if it is a highly disorganized activity (see Online Supplemental Figure 3). Band-pass filtering of ECG signals at the activation frequency of rotors with a driving role (ie, a mother rotor) would accentuate the electrical activity occurring at the passing frequency band by attenuating the effect of electrical activity occurring at other rates and thus allows the detection of atrial SPs at the nearest projected location on the surface. Altogether, we propose that band-pass filtering may allow observing rotational patterns in cases of rotor involvement of large tissue areas and/or a disorganized activity of areas not involved in the rotation maintenance.

Previous studies in which epicardial potentials were reconstructed through the inverse solution formalism reported that rotor activity was rarely seen and accounted for only 15% of patterns observed,[4] although consistently observed in some selected patients.[6] These results are consistent with our observations in raw ECG signals from patients, with 8% of processed maps presenting stable rotors with more than 1 consecutive rotation. Our simulation results show that surface activation patterns do not preserve either the global activation pattern or the shape of activation wavefronts. In fact, patterns observed on the torso surface represent a spatially smoothened version of epicardial propagation. A novel observation in our simulation analysis is that the filaments of epicardial rotors with opposing chiralities, particularly nearby rotors, may join inside the torso and thus those rotors are not detectable on its surface at all, further smoothing complex patterns and importantly suggesting that their epicardial reconstruction through the inverse solution is not attainable. Thus, the ability of surface ECG data to accurately retrieve complex epicardial propagation AF patterns from the patterns on the torso needs to be explored further.

Phase map analysis in surface ECG signals

Phase map analysis applied to surface signals has been proven useful for displaying the propagation pattern projected on the torso. Atrial rotor patterns with the transmural filament, as simulated in our models here, would always produce 2 contralateral axes of extracellular potential rotation, that is, filaments, in the volume conductor (ie, one pointing into the atrial cavity and the other out of the cavity). The intersections of those filaments with the torso surface thus produce 2 SPs: 1 SP at the nearest point on the surface from the epicardial SP (or true SP) and another mirror SP on the opposite side. Surface phase maps in patient data do not always reflect 2 simultaneous SPs because of an incomplete (not geometrically closed) mapping area. Since phase maps are insensitive to the signal power at different locations, both true and mirror SPs look similar. However, spectral analysis at the location

of SPs may allow to discriminate between true and mirror SPs on the basis of the power content at the HDF.

Rotors and dominant frequencies in human AF

Optical mapping both in Langendorff-perfused animal hearts during fibrillation[15] and in monolayers of neonatal rat ventricular myocytes[16] has consistently shown that there is a hierarchical distribution of DF in fibrillating cardiac tissue whereby the fastest regions act as sources driving the slower regions. These high-frequency sources sustain in most cases the AF activity of both atria and may harbor functional rotors. These findings are consistent with EGM analysis of human AF, in which this hierarchical DF pattern has been linked to the existence of drivers at high-frequency sites[1, 13] as well as drifting rotors at sites with transient EGM fractionation.[17] In addition, it has been found that adenosine infusion during AF increases local DFs, particularly at fastest activating sites at baseline, highlighting the hierarchical organization in the DF and the rate of activation of different regions in the atria.[13]

The hierarchical DF patterns can also be detected from surface recordings so that HDF regions can be identified and related to intracardiac DFs and DF gradients.[5] Our results suggest that human AF is driven by rotors most of the time (73%), as they could be detected after HDF filtering. The possible reasons for the absence of rotors during the other 27% of the time are as follows: (1) a rotational pattern was present outside the mapped area, (2) the atrial rotor generates an undetectable signal on the surface, or (3) AF was driven by ectopic foci.

Study limitations

We cannot conclusively confirm that rotational patterns observed in patients correspond to actual atrial rotors, since we do not have simultaneous epicardial and/or endocardial panoramic data. However, we have made use of mathematical models to demonstrate that in case rotors are present during AF on the surface, as we demonstrate in the patients, they are generated by atrial rotors. Although the models of the atria-torso system were simple spherical models, these simple models contain the active and passive volume conductor components needed to gain insight into the mechanisms of visual rotor stabilization by HDF filtering. Insertion of inhomogeneities in the torso model such as lungs do not alter the main conclusions reached here, since they produce a reduction on the surface voltages but not in their morphology (see Online Supplemental Figure 4). In the human torso as well as in a more realistic anatomical model, the projection of epicardial potentials on the surface of the torso will certainly be altered in comparison to those in the spherical models used here and, in particular, certain atrial areas could be masked, but the effects of the volume conductor and band-pass filtering shown here on the torso filaments and the surface SPs should hold. Finally, to reduce ventricular activity from the surface recordings and highlight HDF values, our AF mapping study was performed in the presence of adenosine, which may alter fibrillatory activity and the spatial domain of the rotors in the atria, and potentially alter the sensitivity for their detection of the surface.

Conclusion

Our clinical-computational study suggests that the body surface data on wavebreaks during AF is incomplete, but it contains features that can be linked to reentrant drivers of AF. Narrow band-pass filtering allows selecting the electrical activity projected on the torso at the HDF, which stabilizes the projection of rotors that potentially drive AF on the surface. Phase maps of HDF-filtered surface ECG recordings may allow the noninvasive localization of atrial reentries during AF, enabling further physiologically based rationale for considering the constraints of the inverse solutions. This approach may, therefore, help in planning and performing ablation procedures, decreasing the amount of time required for the search of AF drivers.

Supplementary Material

Refer to Web version on PubMed Central for supplementary material.

Acknowledgment

We appreciate the discussions with Dr Christian Zemlin.

This work was supported in part by the Spanish Society of Cardiology (Becas Investigación Clínica 2009); the Universitat Politècnica de València through its research initiative program; the Generalitat Valenciana grant (ACIF/2013/021); the Ministerio de Economia y Competitividad, Red RIC; the Centro Nacional de Investigaciones Cardiovasculares (proyecto CNIC-13); the Coulter Foundation from the Biomedical Engineering Department, University of Michigan; the Gelman Award from the Cardiovascular Division, University of Michigan; the National Heart, Lung, and Blood Institute grants (P01-HL039707, P01-HL087226, and R01-HL118304); and the Leducq Foundation. Dr Fernández-Avilés served on the advisory board of Medtronic and has received research funding from St Jude Medical Spain. Dr Berenfeld has received research support from Medtronic and St Jude Medical; he is a cofounder and scientific officer of Rhythm Solutions.

ABBREVIATIONS

AF	atrial fibrillation
DF	dominant frequency
ECG	electrocardiogram
EGM	electrogram
HDF	highest dominant frequency
LA	left atrium/atrial
LA-HDF	left atrial highest dominant frequency
RA	right atrium/atrial
RA-HDF	right atrial highest dominant frequency
SP	singularity point

Appendix

Supplementary data

Supplementary data associated with this article can be found in the online version at http://dx.doi.org/10.1016/j.hrthm.2014.05.013.

References

1. Atienza F, Almendral J, Jalife J, Zlochiver S, Ploutz-Snyder R, Torrecilla EG, Arenal A, Kalifa J, Fernández-Avilés F, Berenfeld O. Real-time dominant frequency mapping and ablation of dominant frequency sites in atrial fibrillation with left-to-right frequency gradients predicts long-term maintenance of sinus rhythm. Heart Rhythm. 2009; 6:33–40. [PubMed: 19121797]
2. Narayan SM, Krummen DE, Shivkumar K, Clopton P, Rappel WJ, Miller JM. Treatment of atrial fibrillation by the ablation of localized sources: CONFIRM (Conventional Ablation for Atrial Fibrillation With or Without Focal Impulse and Rotor Modulation) trial. J Am Coll Cardiol. 2012; 60:628–636. [PubMed: 22818076]
3. Guillem MS, Climent AM, Castells F, Husser D, Millet J, Arya A, Piorkowski C, Bollmann A. Noninvasive mapping of human atrial fibrillation. J Cardiovasc Electrophysiol. 2009; 20:507–513. [PubMed: 19017334]
4. Cuculich PS, Wang Y, Lindsay BD, Faddis MN, Schuessler RB, Damiano RJ Jr, Li L, Rudy Y. Noninvasive characterization of epicardial activation in humans with diverse atrial fibrillation patterns. Circulation. 2010; 122:1364–1372. [PubMed: 20855661]
5. Guillem MS, Climent AM, Millet J, Arenal A, Fernández-Avilés F, Jalife J, Atienza F, Berenfeld O. Noninvasive localization of maximal frequency sites of atrial fibrillation by body surface potential mapping. Circ Arrhythm Electro physiol. 2013; 6:294–301.
6. Haissaguerre M, Hocini M, Shah AJ, Derval N, Sacher F, Jais P, Dubois R. Noninvasive panoramic mapping of human atrial fibrillation mechanisms: a feasibility report. J Cardiovasc Electrophysiol. 2013; 24:711–717. [PubMed: 23373588]
7. Berenfeld O, Oral H. The quest for rotors in atrial fibrillation: different nets catch different fishes. Heart Rhythm. 2012; 9:1440–1441. [PubMed: 22521928]
8. Horácek BM, Clements JC. The inverse problem of electrocardiography: a solution in terms of single- and double-layer sources of the epicardial surface. MathBiosci. 1997; 144:119–154.
9. Zlochiver S, Yamazaki M, Kalifa J, Berenfeld O. Rotor meandering contributes to irregularity in electrograms during atrial fibrillation. Heart Rhythm. 2008; 5:846–854. [PubMed: 18534369]
10. Lewis T. Oliver-Sharpey Lectures: on the nature of flutter and fibrillation of the auricle. Br Med J. 1921; 1:590–593. [PubMed: 20770267]
11. Jalife J, Berenfeld O, Mansour M. Mother rotors and fibrillatory conduction: a mechanism of atrial fibrillation. Cardiovasc Res. 2002; 54:204–216. [PubMed: 12062327]
12. Lee S, Sahadevan J, Khrestian CM, Durand DM, Waldo AL. High density mapping of atrial fibrillation during vagal nerve stimulation in the canine heart: restudying the Moe hypothesis. J Cardiovasc Electrophysiol. 2013; 24:328–335. [PubMed: 23210508]
13. Atienza F, Almendral J, Moreno J, et al. Activation of inward rectifier potassium channels accelerates atrial fibrillation in humans: evidence for a reentrant mechanism. Circulation. 2006; 114:2434–2442. [PubMed: 17101853]
14. de Groot NM, Houben RP, Smeets JL, Boersma E, Schotten U, Schalij MJ, Crijns H, Allessie MA. Electropathological substrate of longstanding persistent atrial fibrillation in patients with structural heart disease: epicardial breakthrough. Circulation. 2010; 122:1674–1682. [PubMed: 20937979]
15. Mansour M, Mandapati R, Berenfeld O, Chen J, Samie FH, Jalife J. Left-to-right gradient of atrial frequencies during acute atrial fibrillation in the isolated sheep heart. Circulation. 2001; 103:2631–2636. [PubMed: 11382735]
16. Campbell KF, Calvo CJ, Mironov S, Herron T, Berenfeld O, Jalife J. Spatial gradients in action potential duration created by regional magnetofection of hERG are a substrate for wavebreak and turbulent propagation in cardiomyocyte monolayers. J Physiol. 2012; 590:6363–6379. [PubMed: 23090949]
17. Atienza F, Calvo D, Almendral J, Zlochiver S, Grzeda KR, Martínez-Alzamora N, González-Torrecilla E, Arenal A, Fernández-Avilés F, Berenfeld O. Mechanisms of fractionated

electrograms formation in the posterior left atrium during paroxysmal atrial fibrillation in humans. J Am Coll Cardiol. 2011; 57:1081–1092. [PubMed: 21349400]

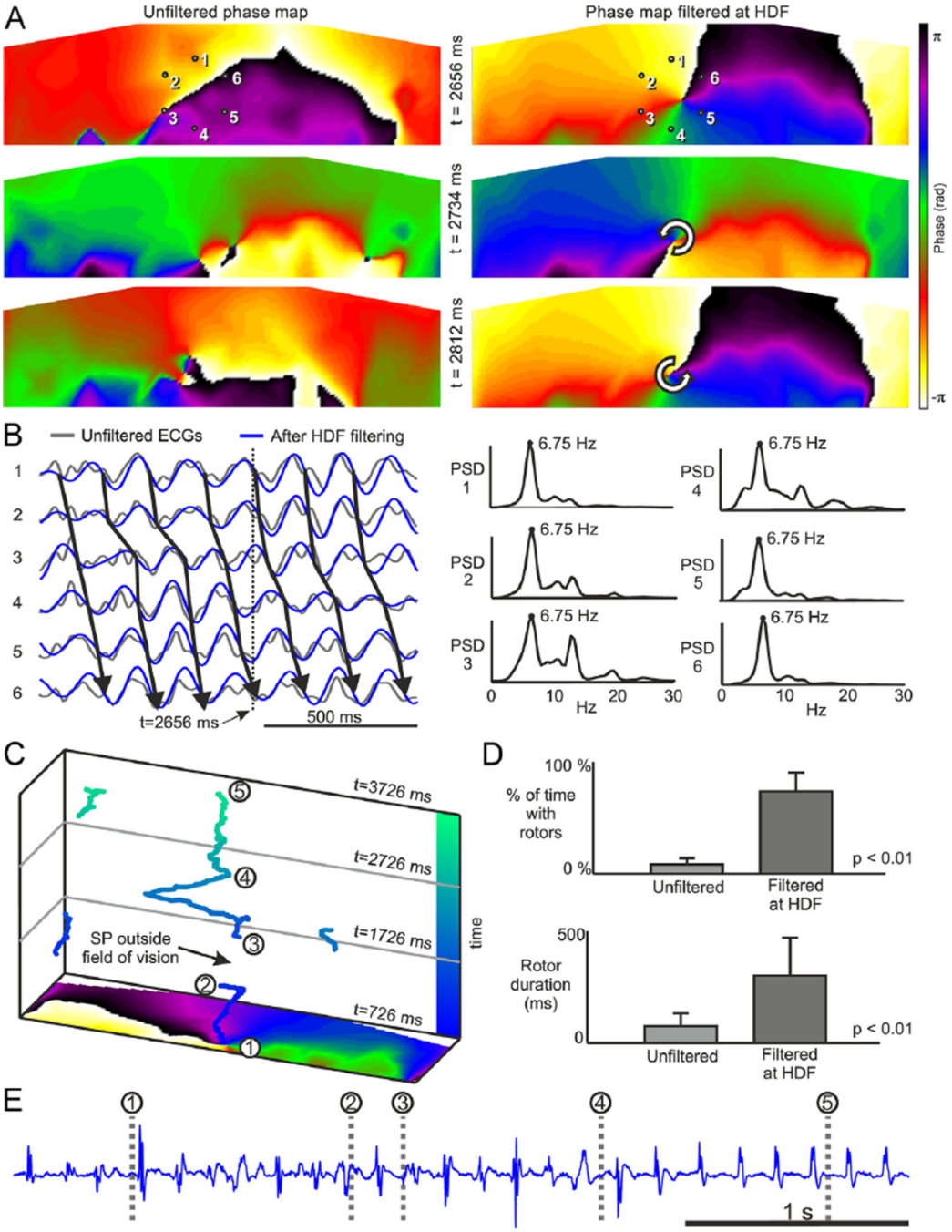

Figure 1.

Surface phase maps during AF. **A:** Surface phase maps at 3 selected times for unfiltered (left) and for HDF-filtered (right) surface potentials. **B:** ECGs at positions 1–6 marked in panel A before and after HDF filtering and PSD for unfiltered ECGs. Time marker at 2656 ms corresponds to the top map in the HDF-filtered data in panel A. **C:** SP trajectories on the torso surface during a 3-second long AF. **D:** Percentage of time with rotors (up) and rotor duration (down) in surface phase maps from unfiltered and HDF-filtered surface potentials over the entire cohort. **E:** Electrogram recorded at the highest DF site in the atria (RSPV)

simultaneously with the surface recordings. AF = atrial fibrillation; DF = dominant frequency; ECG = electrocardiogram; HDF = highest dominant frequency; PSD = power spectral density; RSPV = right superior pulmonary vein; SP = singularity point.

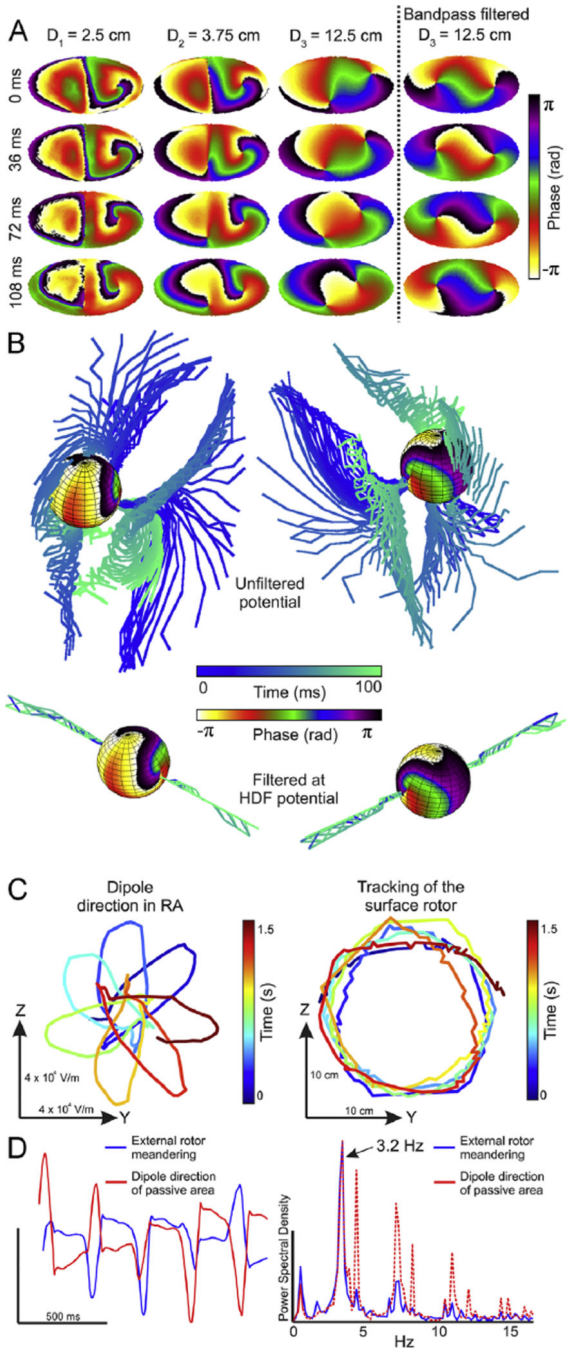

Figure 2.

Epicardial and transition to surface phase maps during AF in a 50% LA-50% RA model. **A:** Phase maps at 4 time instants (top to down) in 3 concentric layers at increasing distances from the epicardium (left to right) and after HDF filtering of surface potentials. **B:** Phase map of epicardial sphere and temporal distribution of filaments for unfiltered potentials and for HDF-filtered potentials. **C:** Tracking of the dipole direction on the RA on the YZ plane (virtual septum plane) and tracking of the surface rotor than arises from the LA without HDF filtering. **D:** Temporal evolution and spectral distribution of the Y coordinate for panel

C. AF = atrial fibrillation; HDF = highest dominant frequency; LA = left atrium/atrial; RA = right atrium/atrial.

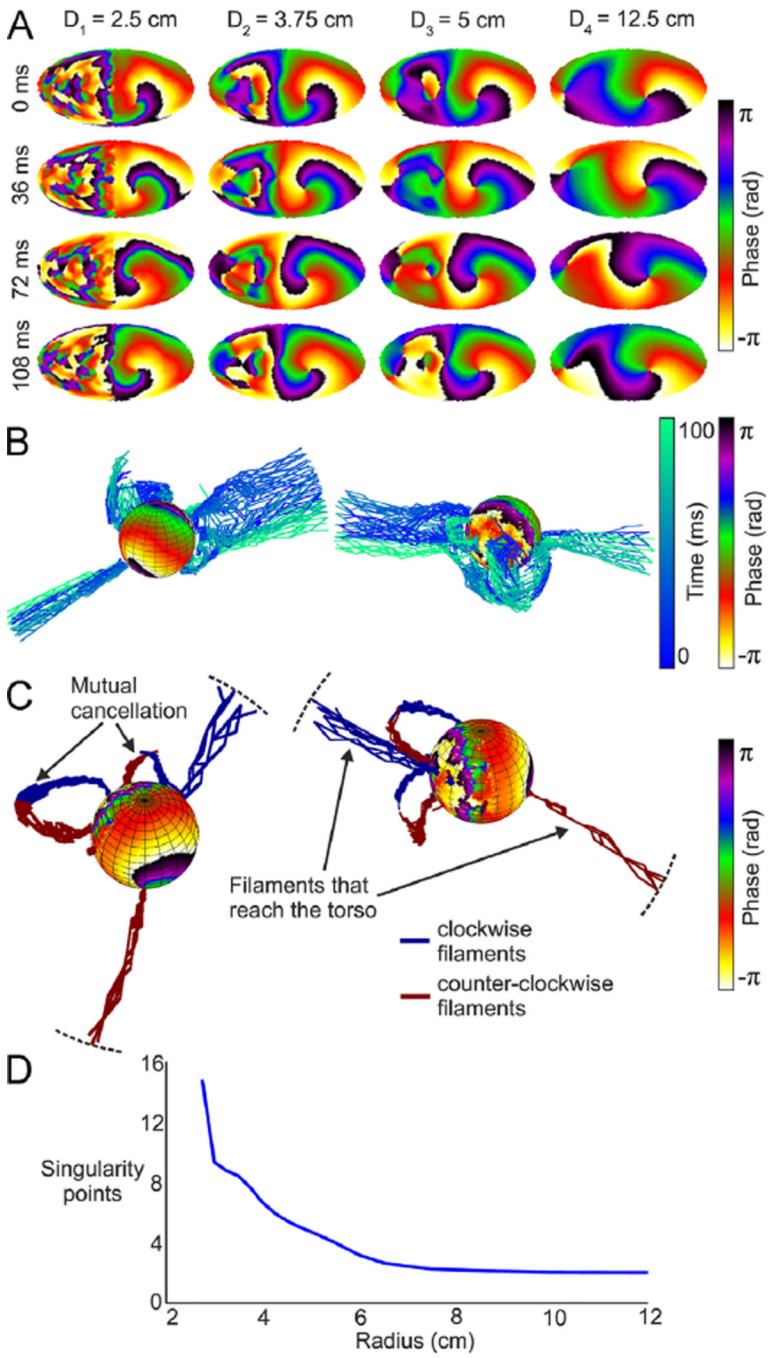

Figure 3.

Epicardial and transition to surface phase maps during AF in a 50% LA-50% fibrosis atrial model. **A:** Phase maps at 4 time instants (top to down) in 4 concentric layers at increasing distances from the epicardium (left to right). **B:** Phase map of the epicardial sphere and temporal evolution of filaments for unfiltered potentials. **C:** Phase map of epicardial sphere and distribution of filaments (clockwise rotations in blue; counterclockwise rotations in red) inside the torso during 10 ms. D: Average number of rotors per frame. AF = atrial fibrillation; LA = left atrial.

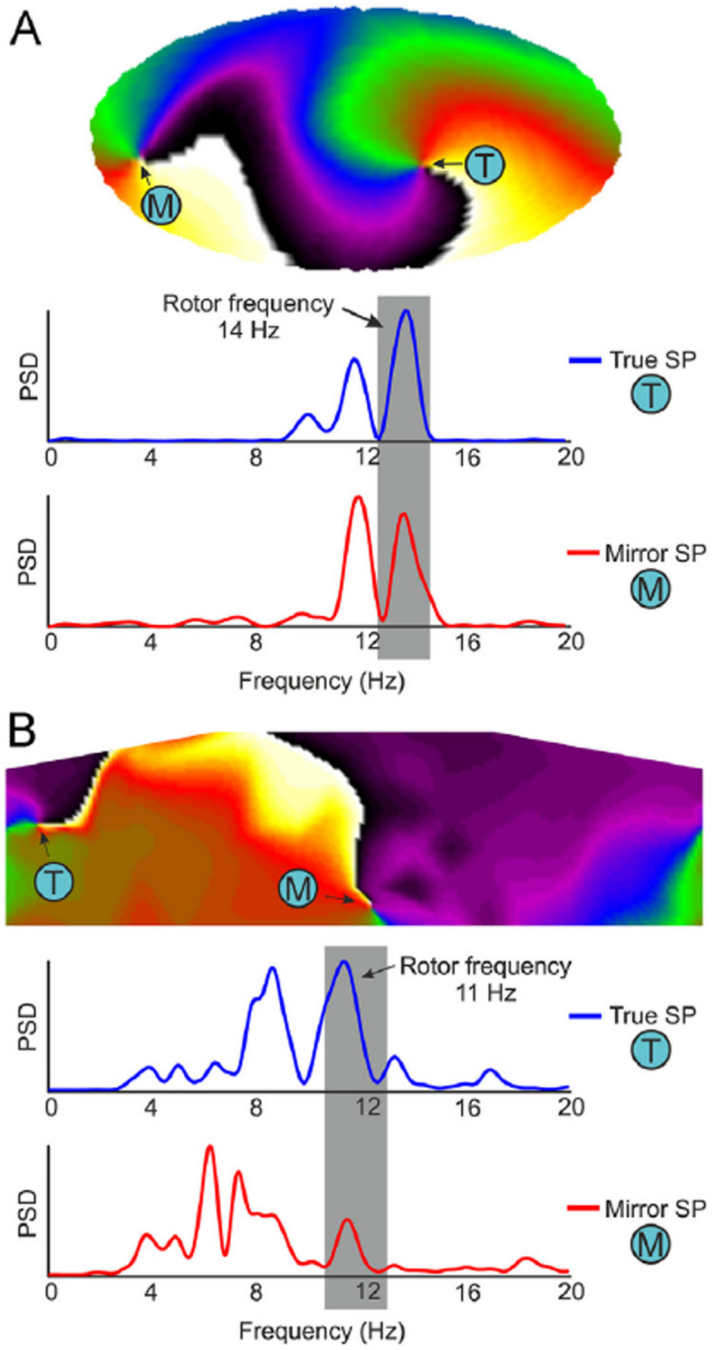

Figure 4.

Discrimination of true and mirror SPs at surface phase maps in a simulated and human AF. **A:** Surface phase map in a 50% LA-50% fibrosis atrial model and power spectra of surface potentials at the true rotor location (blue, T) and at the mirror rotor location (red, M). **B:** Surface phase map after HDF-filtering from patient 11 during AF and power spectra of surface potentials before the filtering at the true rotor location (blue, T) and at the mirror rotor location (red, M). AF = atrial fibrillation; HDF = highest dominant frequency; LA = left atrial; PSD = power spectral density; SP = singularity point.

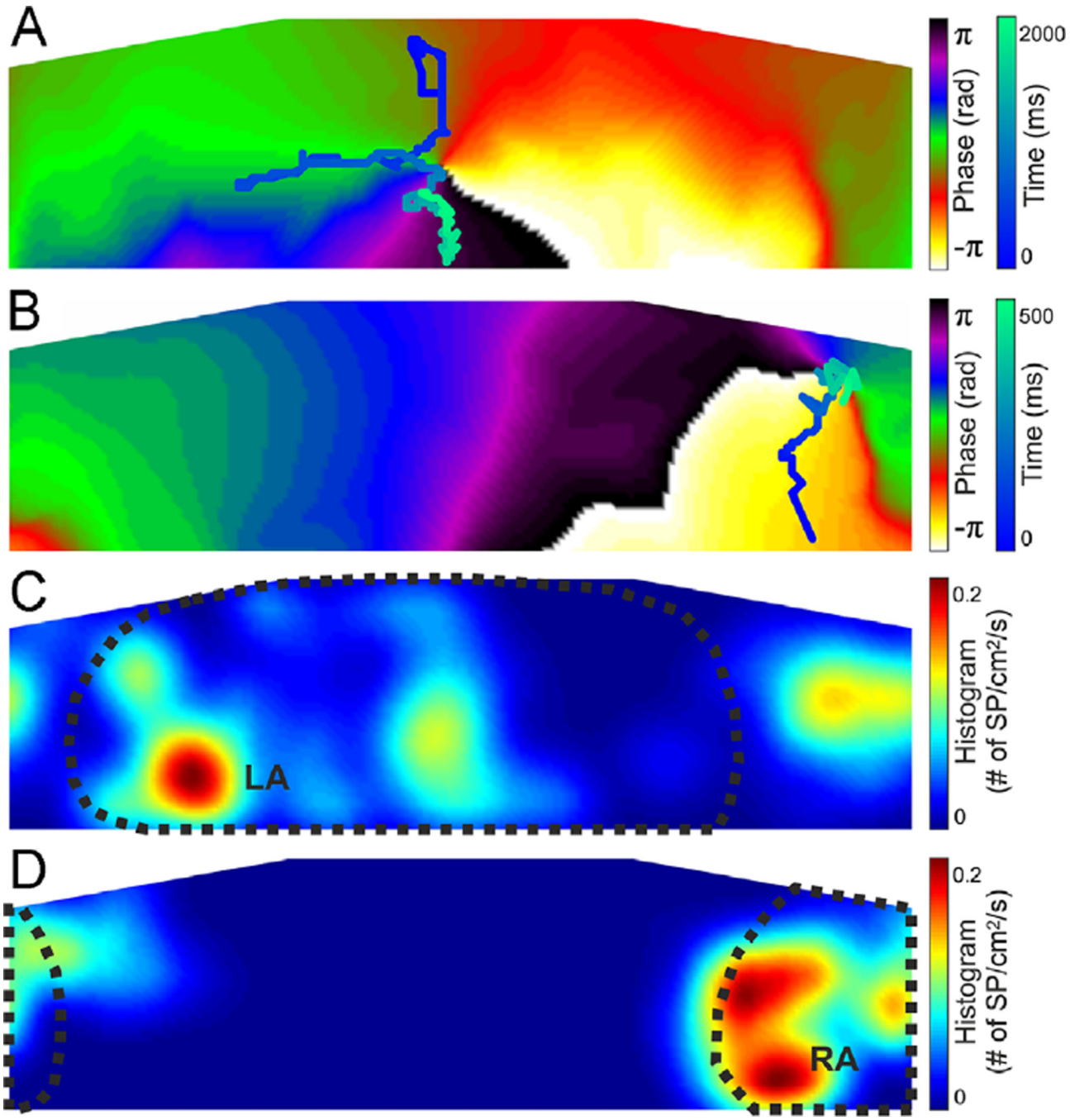

Figure 5.

Spatial distribution of surface rotors in human AF. **A:** Phase map and rotor tracking (blue scale) after LA-HDF filtering in an LA-fastest patient. **B:** Phase map and rotor tracking (blue scale) after RA-HDF filtering in an RA-fastest patient. **C:** Histogram of the rotor position for all rotors detected in patients with an interatrial DF gradient after LA-HDF filtering. LA-detected region is outlined with a dotted line. **D:** Histogram of the rotor position for all rotors detected in patients with an interatrial DF gradient after RA-HDF filtering. RA-detected region is outlined with a dotted line. AF = atrial fibrillation; DF =

dominant frequency; LA = left atrial; LA-HDF = left atrial highest dominant frequency; RA = right atrial; RA-HDF = right atrial highest dominant frequency; SP = singularity point.